Calibration-free wavelength-modulation spectroscopy for measurements of gas temperature and concentration in harsh environments

Gregory B. Rieker,* Jay B. Jeffries, and Ronald K. Hanson

High Temperature Gasdynamics Laboratory, Department of Mechanical Engineering, Stanford University, Stanford, California 94305, USA

*Corresponding author: grieker@stanfordalumni.org

Received 15 June 2009; revised 1 September 2009; accepted 3 September 2009; posted 8 September 2009 (Doc. ID 112682); published 5 October 2009

We present a practical implementation of calibration-free wavelength-modulation spectroscopy with second harmonic detection (WMS-2f) for measurements of gas temperature and concentration in harsh environments. The method is applicable to measurements using lasers with synchronous wavelength and intensity modulation (such as injection current-tuned diode lasers). The key factors that enable measurements without the on-site calibration normally associated with WMS are (1) normalization of the WMS-2f signal by the first harmonic (1f) signal to account for laser intensity, and (2) the inclusion of laser-specific tuning characteristics in the spectral-absorption model that is used to compare with measured 1f-normalized, WMS-2f signals to infer gas properties. The uncertainties associated with the calibration-free WMS method are discussed, with particular emphasis on the influence of pressure and optical depth on the WMS signals. Many of these uncertainties are also applicable to calibrated WMS measurements. An example experimental setup that combines six tunable diode laser sources between 1.3 and 2.0 μm into one probe beam for measurements of temperature, H_2O, and CO_2 is shown. A hybrid combination of wavelength and frequency demultiplexing is used to distinguish among the laser signals, and the optimal set of laser-modulation waveforms is presented. The system is demonstrated in the harsh environment of a ground-test scramjet combustor. A comparison of direct absorption and 1f-normalized, WMS-2f shows a factor of 4 increase in signal-to-noise ratio with the WMS technique for measurements of CO_2 in the supersonic flow. Multidimensional computational fluid-dynamics (CFD) calculations are compared with measurements of temperature and H_2O using a simple method that accounts for the influence of line-of-sight (LOS) nonuniformity on the absorption measurements. The comparisons show the ability of the LOS calibration-free technique to gain useful information about multidimensional CFD models.

OCIS codes: 120.1740, 120.6780, 300.1030, 300.6380, 300.6280.

1. Introduction

Over the last 35 years, tunable diode laser-absorption spectroscopy (TDLAS) has matured into a robust and convenient means of measuring a wide variety of gas parameters in difficult, real-world environments [1–7]. Light emitted from tunable diode sources is passed through a gaseous test sample to a detector, and the absorption of light can be related to gas temperature, pressure, species concentration, and velocity using spectral-absorption models for the target absorbing species.

For target species with discrete spectral-absorption features (e.g., small molecules and atoms), where the absorption is wavelength dependent over a short spectral window (a few cm^{-1}), the laser wavelength can be modulated sinusoidally and the nonuniform absorption gives rise to components in the detector signal at the harmonics of the original sinusoid frequency. The harmonic signals can be isolated with lock-in amplifiers (essentially bandpass filters),

0003-6935/09/295546-15$15.00/0

which greatly reduce the influence of laser and electronic noise by filtering out components of the detector signal outside of the harmonics. The harmonic signals can then be related back to the spectral-absorption models for the target species and used to infer gas properties, but with much higher sensitivity than direct-absorption measurements.

Modulation spectroscopy is divided into two categories. The first is frequency modulation spectroscopy (FMS), in which the modulation frequency [8] is greater than the optical frequency linewidth of the probed absorption feature (100 MHz to the several gigahertz range). The second category is wavelength-modulation spectroscopy (WMS), in which the modulation frequency is much less than the optical frequency linewidth of the probed absorption feature (kilohertz to several megahertz range). A good overview and comparison of the two categories can be found in companion papers by Silver [9] and Bomse *et al.* [10], who found that high-frequency WMS (>100 kHz) offers excellent sensitivity without the burden of extremely fast detection electronics, as required by FMS. This is an important consideration for practical, field-deployable systems, which are the concern of this paper.

Recognizing the power of WMS for highly sensitive measurements, many researchers have applied the technique to enable measurements in harsh environments that otherwise might not be possible with direct-absorption spectroscopy. Measurements in a high-pressure coal combustor [11], ground-test scramjet engines [12,13], internal combustion engines [14], and a variety of trace gas situations ([15] and references therein) are just a few examples using WMS. A handheld methane leak detector [16] and combustion measurements in a microgravity drop tower [17] are excellent examples of portable WMS systems where the sensor hardware itself is also compact, robust, and capable of operating in difficult environments.

One of the key drawbacks to applying traditional WMS in practical environments for temperature and concentration measurements is the need to calibrate the WMS signals to a known mixture and condition (or a direct measurement of absorption) in order to recover the absolute concentration or temperature. For most real-world environments and field-deployable sensors, this is difficult and impractical, and may involve the need for additional equipment and complexity in the sensor system. Several researchers have proposed methods to enable "calibration-free" measurements using WMS. In this paper, we define "calibration free" as a method that enables absolute measurements of temperature or concentration without on-site calibration or comparison with a known mixture or condition. It should be pointed out immediately that, like most absorption-based measurements (e.g., [18]), characterization of the probe lasers and certain spectral parameters (such as line strength and pressure broadening of the target absorption feature) are still necessary for "calibration-free" WMS.

Henningsen and Simonsen [19] proposed a method that relates various parameters of the second harmonic ($2f$) signal, such as the peak-to-trough ratio and the line width, to develop algorithms that infer absolute species concentration, provided that the pressure, path length, and temperature in the environment are known. This method is useful for certain cases where many of the environmental conditions are known. However, the method also requires that the absorption feature is completely isolated (so there is no distortion to any part of the line shape or wings), and that the laser can be tuned completely across the absorption feature such that the nonabsorbing region on either side of the feature can be used to extract the laser intensity to normalize the signal. This is difficult in practical environments, which often comprise gas mixtures that contain interfering species, such as H_2O and elevated pressures where pressure broadening expands the feature beyond the scan range of the laser. If H_2O itself is the target molecule, finding an isolated transition is difficult among the many overlapping transitions, even at room temperature.

Duffin *et al.* developed a form of WMS that recovers the direct-absorption line shape from the first harmonic ($1f$) signal for measurements of concentration and pressure [20,21]. This method is useful in that traditional direct-absorption data reduction methods can be applied once the direct-absorption line shape is obtained; however, for application in harsh environments, the method has several potential drawbacks. The technique works well for small modulation amplitudes when the harmonic line shapes closely approximate the derivatives of the direct-absorption line shape but, when the modulation amplitude is increased to maximize the harmonic signals (which is necessary in harsh environments to obtain sufficient SNR), the analysis becomes more complicated. In addition, the technique also requires that the laser scan across the entire absorption feature to recover a nonabsorbing baseline to normalize for laser intensity, which is difficult for the same reasons listed in the previous paragraph.

The calibration-free WMS method we focus on in this paper uses the $2f$ signal to gain absorption information, and is applicable to any WMS light source that exhibits synchronous wavelength and intensity modulation (such as an injection-current-tuned diode laser). Cassidy and Reid [22] first recognized that, for these types of light sources, the $1f$ signal can be used to normalize the $2f$ signal for variations in laser intensity. This property has since been successfully exploited by several authors [11,16,23,24]. It was recently suggested in Li *et al.* [25] that combining this intensity normalization with a model for the WMS signals based on the specific laser tuning characteristics for the probe laser and spectral data measured in the laboratory or obtained from HITRAN [26] eliminates all calibration factors between

experiment and model. The experiment and model can thus be directly compared, as shown in [27,28], and this comparison can be used to infer temperature and species concentration, as first demonstrated in [14,29]. This method works at any pressure where a 2*f* signal can be obtained, works with congested spectra so long as spectral information for the neighboring features is included in the model, and is applicable at any modulation depth. In addition, the method does not require that the laser scan across the entire feature—only the 2*f* peak must be captured—which is helpful at high pressures and, as will be shown later, is desirable when using frequency demultiplexing of WMS signals from different lasers impinging on one detector. The method does have intricacies, such as different optimal implementations depending on the environment and conditions, and drawbacks, such as the need for knowledge of the gas pressure in the probe region. This paper seeks to study these topics for calibration-free WMS and present a helpful framework for setting up calibration-free WMS measurements in harsh environments.

Specifically, this paper seeks to achieve four goals.

1. **Clearly describe how calibration-free WMS is performed.** The focus of this section will not be on the WMS models themselves, which have been developed and described elsewhere [25]. Rather, the focus will be a discussion of the practical implementation of the measurement and model such that they can be compared to infer gas properties.
2. **Study the uncertainties involved with WMS, particularly as applied to harsh environments.** Particular focus will be placed on understanding the effect of pressure uncertainties and nonuniformities along the laser line of sight (LOS), and the effects of modulation amplitude and optical thickness on uncertainty.
3. **Describe the current state-of-the-art calibration-free WMS system used in our laboratory.** The system involves hybrid demultiplexing—using both wavelength and modulation frequency multiplexing to combine six lasers with wavelengths ranging from 1.3 to 2.0 μm in a single probe beam and later distinguish their signals.
4. **Demonstrate this WMS system for measurements of temperature, H_2O, and CO_2 in a scramjet test facility.** The system is demonstrated for measurements of CO_2 concentration in a supersonic vitiated flow in a model scramjet combustor at the Air Force Research Laboratory (AFRL) at Wright-Patterson Air Force Base (WPAFB) [30]. Comparisons between direct-absorption and WMS measurements in the same environment show a 4× increase in signal-to-noise ratio (SNR) with WMS, even though the measurement is not limited by laser noise (a situation where WMS shows an even greater improvement over direct absorption).

In addition, a simple method that takes into account gas nonuniformities along the laser LOS is used to compare measurements of temperature and H_2O with two-dimensional (2D) CFD calculations during full scramjet combustor operation. An expected WMS signal is calculated from the multidimensional CFD and is used to infer an expected laser-measured LOS temperature and H_2O concentration. This value, which is slightly different than the simple path-average temperature and H_2O concentration, can be directly compared to the laser measurement to yield useful information about both scramjet combustor and CFD model performance.

2. Calibration-Free Wavelength-Modulation Spectroscopy

This section is divided into three parts—Subsection 2.A describes the WMS measurement, Subsection 2.B briefly describes the WMS model, and Subsection 2.C discusses how to extract gas properties from the comparison of model and measurement.

A. Wavelength-Modulation Spectroscopy Measurement

Figure 1 shows a schematic of a scanned-wavelength WMS measurement using a diode laser. Much like traditional scanned-wavelength direct-absorption

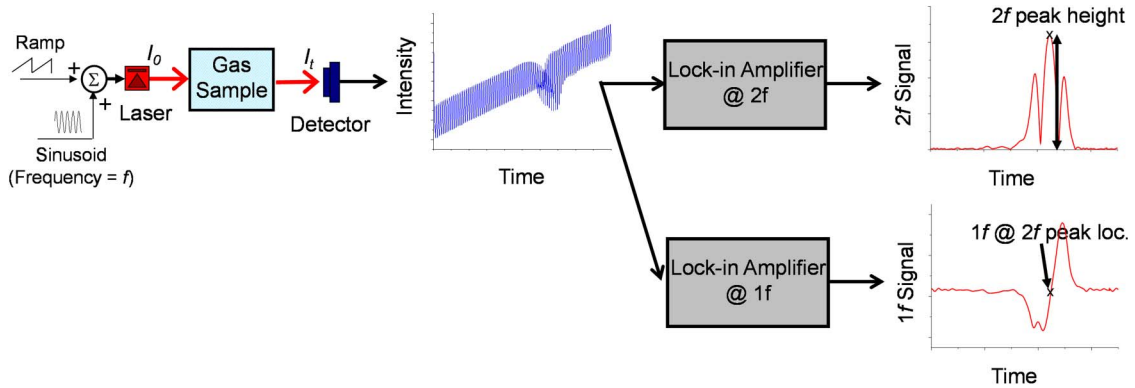

Fig. 1. (Color online) Schematic of WMS (1*f*-normalized, WMS-2*f*). Example data is water-vapor absorption measured in the scramjet combustor at WPAFB (see Sections 5 and 6). The 2*f* signal is always positive due to the phase-insensitive lock-in approach taken in these experiments (described in Subsection 2.A). The slight distortion on the left side of the primary absorption feature is caused by a second, smaller absorption feature.

measurements, the diode laser injection current is tuned with a repetitive ramp waveform. This has the effect of repetitively ramping the laser intensity and the laser wavelength across the absorption feature. Unlike traditional direct absorption, however, an additional high-frequency sinusoid is superimposed on the repetitive injection current ramp to generate an additional high-frequency modulation in both the laser intensity and wavelength. When the laser wavelength is tuned across an absorption feature (e.g., by the repetitive ramp), the high-frequency wavelength modulation causes the laser to scan back and forth over part of the absorption feature twice per modulation cycle. Absorption thus affects the shape of the transmitted laser intensity and introduces harmonic components to the detected signal. An example detector signal (intensity versus time) is shown in Fig. 1.

The detector signal is passed to several digital lock-in amplifiers to isolate the first harmonic ($1f$) and the second harmonic ($2f$) signals. The lock-in amplifiers act by multiplying the detector signal by a reference sinusoid at the frequency of interest ($1f$ or $2f$) to take advantage of the trigonometric identity, $\cos(\alpha)\cos(\beta) = \frac{1}{2}\cos(\alpha-\beta) + \frac{1}{2}\cos(\alpha+\beta)$, to shift the harmonic components at the frequency of interest to DC [31]. A low-pass filter is then applied to isolate the DC value and eliminate all components outside of the filter bandwidth [32].

In order to compare the WMS measurements to the model presented in Subsection 2.B, it is important to either tune the phase of the lock-in reference sinusoid to precisely match the phase of the detected harmonic signal, or to use a phase-insensitive lock-in approach. In our laboratory, we use the phase-insensitive approach by passing the detector signal in parallel through two lock-ins for each harmonic. One lock-in multiplies the detector signal by a reference sine wave (recovering what we refer to as the Y component of the signal) and the other multiplies the detector signal by a reference cosine wave (recovering what we refer to as the X component of the signal). The root-sum square of the X and Y components is the total magnitude of the harmonic component, regardless of the phase shift between the detector signal and lock-ins. The root-sum square is always positive, and causes the $2f$ peak and wing lobes to have the same sign (they have opposite signs if the traditional lock-in approach is taken).

There are several sources of $2f$ background signals that must be avoided or subtracted from the experimental measurements before the measurements can be directly compared with the model presented in Subsection 2.B. The sources fall into three categories: background signals induced by etalon effects along the light path, background signals induced by nonlinear intensity modulation effects in the laser, and background absorption by gases outside the measurement volume.

Etalon effects are caused by constructive/destructive interference arising from internal reflections off parallel faces in the optical path. Their wavelength-dependent nature can induce spurious $2f$ signals [33]. These effects must be avoided in the optical design of the sensor system because they are often unstable and, therefore, cannot be successfully subtracted from the measured $2f$ signal or included in the WMS model. We have found that the use of angle-polished fibers and a 1° to 3° wedge on the face of all windows along the light path is sufficient to reduce the contributions of etalons below that of other noise sources in most harsh environments. This approach complicates alignment slightly, but has achieved good results for a variety of window thicknesses and incident beam diameters. For applications in which a wedged window is not feasible, it is also possible to use a thick window with an off-normal beam incidence.

Nonlinear intensity modulation effects induce extra components in the absorption-dependent portion of the $2f$ signal as well as an additional component in the $2f$ signal in the absence of absorption. Both effects are included in the model presented in Subsection 2.B, but the latter must be subtracted from the measured (and simulated) $2f$ signal in order to maintain a linear relationship between the $2f$ signal and species concentration (see Subsection 2.C).

Finally, it is best to minimize background absorption by gases outside of the desired measurement volume (for example, between the detector and the outside window to a high-temperature measurement environment). If background absorption cannot be avoided, it must be held stable, measured, and subtracted prior to comparison between measurement and model. For the measurements described later in the paper, regions of the laser path outside the scramjet combustor were purged with a continuous, regulated flow of nitrogen, which greatly reduced background absorption. The remaining absorption was confirmed to be steady over the period of the experiments, measured, and then subtracted as outlined in the next paragraph.

If background subtraction is necessary (because background absorption and/or nonlinear intensity modulation effects are present), the measured $2f$ signal and background must be normalized for laser intensity (using the $1f$ signal) and then the vector subtracted. The process is described by the equation

$$2f/1f = \sqrt{\left[\left(\frac{X_{2f}}{R_{1f}}\right)_{\text{raw}} - \left(\frac{X_{2f}}{R_{1f}}\right)_{\text{bg}}\right]^2 + \left[\left(\frac{Y_{2f}}{R_{1f}}\right)_{\text{raw}} - \left(\frac{Y_{2f}}{R_{1f}}\right)_{\text{bg}}\right]^2}. \quad (1)$$

Following the notation of [25], X_{2f} and Y_{2f} refer to the X and Y components of the lock-in outputs at $2f$, and R_{1f} refers to the root-sum-square magnitude of the X and Y components of the lock-in outputs at $1f$. The subscripts "raw" and "bg" refer to the raw WMS signal (i.e., that which contains contributions from both the absorption signal of interest and the background signals), and the background signal (i.e., that which is measured with the intended measurement region purged or otherwise eliminated from the optical path). Note that, if background absorption is not present, the background signal due to nonlinear intensity modulation effects can be simulated using the model in Subsection 2.B, and then used in place of a measured background in Eq. (1).

B. Wavelength-Modulation Spectroscopy Model

The WMS model used here is based on Li *et al.* [25], and has been verified experimentally on H_2O and CO_2 absorption with different diode lasers, modulation amplitudes and frequencies, and at a variety of pressures up to 30 atm and temperatures up to 900 K [27–29]. This model extends the work of many researchers [9,11,33–38], to include laser-specific tuning characteristics. Here, the model is further extended to be compatible with any optical depth (the model in [25] assumes an optically thin medium). Combining this laser-specific model with intensity normalization of the $2f$ signal by the $1f$ signal creates a system in which the model and measurement can be directly compared without calibration to infer absolute gas properties.

The model is created by simulating the process that occurs in the experiment. First, the incident laser intensity and wavelength-dependent absorption must be modeled. The incident laser intensity is modeled by

$$I_0(t) = \bar{I}_0[1 + i_0\cos(\omega t + \psi_1) + i_2\cos(2\omega t + \psi_2)], \quad (2)$$

where $\bar{I}_0$ is the average laser intensity, i_0 and i_2 are the amplitudes of the linear and the first term of the nonlinear laser intensity modulation (normalized by $\bar{I}_0$), and ψ_1 and ψ_2 are the phase shifts between the laser intensity modulation and frequency (wavelength) modulation for linear and nonlinear intensity modulation, respectively. Each of the parameters i_0, i_2, ψ_1, and ψ_2 must be measured in the laboratory according to the procedures in [25] for the laser and laser operation settings (injection current, modulation frequency, etc.) that are to be used for the measurements. If a repetitive ramp injection current is used in addition to the high-frequency sinusoidal modulation to scan the laser across the absorption feature (as described in Subsection 2.A), the value of $\bar{I}_0$ and, therefore, the values of i_0 and i_2, change throughout the scan. In this case, the named laser parameters should be measured at the point in the repetitive ramp that corresponds to the $2f$ peak, as this is the only part of the scan that is compared with the model.

Absorption is simulated by defining a transmission coefficient for the laser light through the absorbing medium [which depends on the laser frequency (wavelength)] in terms of a Fourier series:

$$\tau(\nu(t)) = \sum_{k=0}^{k=+\infty} H_k(\bar{\nu}, a)\cos(k\omega t), \quad (3)$$

where $\nu(t) = \bar{\nu} + a\cos(\omega t)$ is the instantaneous laser frequency (wavelength), $\bar{\nu}$ is the average laser frequency (wavelength), and a is the amplitude of the frequency (wavelength) modulation. The parameters $\bar{\nu}$ and a must be measured for the specific laser and laser operation procedures used for the measurements (see [25] for details). Combining this with the Beer–Lambert relation, the H terms can be defined as

$$H_0(T, P_i, \bar{\upsilon}, a) = \frac{1}{2\pi}\int_{-\pi}^{\pi} \exp\left\{-\sum_j S_j(T)\cdot\phi_j(T, P, x, \bar{\upsilon} + a\cos\theta)\cdot P\cdot x_i\cdot L\right\} d\theta, \quad (4)$$

$$H_k(T, P_i, \bar{\upsilon}, a) = \frac{1}{\pi}\int_{-\pi}^{\pi} \exp\left\{-\sum_j S_j(T)\cdot\phi_j(T, P, x, \bar{\upsilon} + a\cos\theta)\cdot P\cdot x_i\cdot L\right\} \cos k\theta d\theta, \quad (5)$$

where $S_j(T)$ is the line strength at temperature T of absorption transition j, P is the total pressure, x_i is the mole fraction of the absorbing species i, L is the path length of laser beam travel through the absorbing medium, and ϕ_j is the line-shape function of transition j. Depending on the experimental conditions, the line-shape function can be modeled with a Gaussian, Voigt, or Lorentzian profile using broadening parameters that are known either through careful laboratory measurements of the type shown in [39] or from HITRAN [26]. The line strength also must be known in order to calculate the H terms, and can be obtained through these same sources.

The detector signal is then modeled by multiplying the incident laser intensity Eq. (2) with the first few terms of the transmission function Eq. (3). To simulate the X and Y components of the phase-insensitive lock-ins tuned to measure the $2f$ signal, the detector signal is multiplied by $\cos(2\omega t)$ and $\sin(2\omega t)$, respectively. Only DC terms are carried after the multiplication to simulate the effect of the low-pass filtering step of the lock-in:

$$X_{2f} = \frac{G\bar{I}_o}{2}\left(H_2 + \frac{i_o}{2}(H_1 + H_3)\cos\psi_1 + i_2\left(H_o + \frac{H_4}{2}\right)\cos\psi_2\right), \quad (6)$$

$$Y_{2f} = -\frac{G\bar{I}_o}{2}\left(\frac{i_o}{2}(H_1 - H_3)\sin\psi_1 + i_2\left(H_o - \frac{H_4}{2}\right)\sin\psi_2\right). \quad (7)$$

G is the electro-optical gain of the detection system. It does not need to be known or measured since normalization with the $1f$ signal in the next step cancels this term.

Using the same method but changing the lock-in reference signals to $\cos(\omega t)$ and $\sin(\omega t)$, the components of the $1f$ signal can be calculated:

$$X_{1f} = \frac{G\bar{I}_o}{2}\left[H_1 + i_o\left(H_0 + \frac{H_2}{2}\right)\cos\psi_1 + \frac{i_2}{2}\left(H_1 + H_3\right)\cos\psi_2\right], \quad (8)$$

$$Y_{1f} = -\frac{G\bar{I}_o}{2}\left[i_0\left(H_0 - \frac{H_2}{2}\right)\sin\psi_1 + \frac{i_2}{2}\left(H_1 - H_3\right)\sin\psi_2\right]. \quad (9)$$

The $1f$ magnitude is then calculated using the root-sum square:

$$R_{1f} = \sqrt{{X_{1f}}^2 + {Y_{1f}}^2}.$$

We are now able to completely simulate the $1f$ and $2f$ signals. With knowledge of the specific laser tuning characteristics and the specific spectral parameters for the target absorption transition, the H terms can be directly calculated from Eqs. (4) and (5). We can then calculate the X and Y components of the $1f$ and $2f$ signals using Eqs. (6)–(9) (omitting the $G\bar{I}_0/2$ term, since it cancels when the two signals are divided). The final step is to compute the background-subtracted $2f/1f$ signal. Here, we also use Eq. (1) so that our simulations mirror our experiment. The "raw" and "bg" terms from Eq. (1) are simply replaced with the simulation with and without absorption.

One should note that this model is valid for any optical thickness, for any modulation amplitude or laser operating conditions, for any environmental condition (T, P, x), and for spectra with overlapping interference from neighboring features.

C. Comparison of Wavelength-Modulation Spectroscopy Model and Measurement to Infer Gas Temperature and Concentration

The method presented here assumes that both the gas temperature and the absorbing species concentration are unknown along the laser LOS, which is typical of many practical applications. In this method, the WMS signals from two absorption features will be used to infer the LOS-average temperature and species concentration along the beam path. The effects of nonuniform gas property distributions along the LOS will be discussed in Section 6.

To understand the dependence of the $2f/1f$ signal on gas properties, it is easiest to simplify the full model presented in Subsection 2.B for an optically thin (absorbance <0.05) line-center measurement of an isolated absorption transition. Assuming linear intensity modulation with a phase shift of π, the $1f$-normalized $2f$ signal simplifies to

$$2f/1f \approx \frac{H_2}{i_0} = \frac{S(T)\cdot P\cdot x_i\cdot L}{i_0\cdot\pi}\int_{-\pi}^{\pi}\phi(\bar{\upsilon}_{\text{peak}} + a\cos\theta)\cos 2\theta \mathrm{d}\theta. \quad (10)$$

Taking the ratio of the $2f/1f$ signals from two different absorption features cancels the direct dependence on species concentration:

$$\text{Ratio} = \frac{i_{0,2}}{i_{0,1}}\frac{S(T)_1}{S(T)_2}\frac{\int_{-\pi}^{\pi}\phi_1(\bar{\upsilon}_{\text{peak}} + a\cos\theta)\cos 2\theta \mathrm{d}\theta}{\int_{-\pi}^{\pi}\phi_2(\bar{\upsilon}_{\text{peak}} + a\cos\theta)\cos 2\theta \mathrm{d}\theta}. \quad (11)$$

The ratio of $i_{0,i}$ terms is a constant, the ratio of line strengths depends solely on T, and the ratio of line-shape integrals depends weakly on T and on x_i and P for cases where the Voigt or Lorentzian profiles are used. The dependence on pressure of the line-shape integral is the subject of Section 3, as it can be minimized through the judicious selection of absorption features and laser-modulation parameters. However, to maximize the accuracy of the measurement, it is important to simultaneously measure pressure in the probed region in order to correctly calculate the expected ratio. The ratio of $2f/1f$ signals is thus calculated for a range of temperatures at the measured pressure and at a nominal expected value of x_i. The simulated ratio is compared directly with the measured ratio to infer the temperature.

Next, the species partial pressure or mole fraction is inferred using the $2f/1f$ signal for one absorption feature. With the temperature now known, Eq. (10) can be used to determine the concentration through the following relationship:

$$P_{i,\text{meas.}} = \frac{(2f/1f)_{\text{meas.}}}{(2f/1f)_{\text{sim.}}}\cdot P_{i,\text{sim.}} \quad (12)$$

If the pressure is well known, then P_i can be replaced with x_i to calculate the mole fraction directly. For cases where the Voigt or Lorentzian line shapes are used, the line-shape integral has some dependence on species concentration through the dependence of pressure broadening on the collision partner. For these cases, if the absorbing species is a significant

portion of the gas mixture (e.g., >5%) and the measured species concentration using Eq. (12) is significantly different from the nominal species concentration used for the simulations (see Subsection 3.B and Fig. 5), it is necessary to iterate using the measured species concentration to resimulate the $2f/1f$ signals and subsequently recalculate the measured temperature and species concentration.

For cases where any of the simplifying assumptions applied above are not valid, the same procedure is followed using the full model equations presented in Subsection 2.B. Using the full equations refines the simulated signals and ratios, but does not significantly change the dependences described above. Two important points to note for cases where the absorbance levels fall outside the optically thin limit: the $1f$ signal is somewhat affected by absorption, and Eq. (12) is not valid for large deviations between the simulated and measured conditions (see Subsection 3.B). For these cases, it therefore becomes important for the simulated concentration to more closely match the measured concentration (which may require iteration).

3. Analysis of Uncertainty in 2f Measurements

The potential sources of uncertainty in calibration-free WMS are summarized and explained in Table 1. In this section we focus specifically on source 7, measurement uncertainty induced by pressure deviation between the simulated and experimental conditions, and source 8, uncertainty in concentration measurements induced by optical depth. Source 7 is particularly relevant to WMS sensors developed for harsh, practical applications where the pressure may be uncertain, difficult to measure accurately with a transducer, and/or varying along the laser LOS. Source 8 is important for sensors developed for harsh environments because it is often desirable in these environments to use strong absorption features (that exceed the linear optically thin limit) to increase signal levels and improve SNR. These two sources have not received much attention in the literature.

A. Pressure Uncertainty

In this section, we focus on the effect of pressure on the $2f$ signal to understand the effect that pressure uncertainties will have on measurements of temperature and concentration. Since we focus primarily on the $2f$ signal, the figures and conclusions drawn in this section are also applicable to calibrated WMS measurements where the pressure changes from the value at which the signals were calibrated.

The effect of pressure on the $2f$ signal is most easily seen in the simplified case of the $2f$ signal in Eq. (10). The signal is directly proportional to the absorbing species partial pressure (which is the ideal

Table 1. Summary of Potential Sources of Uncertainty in Calibration-Free WMS

Source of Uncertainty	Description	Mitigation
1. Spectral parameters	Absorption-feature line strength, line broadening, and broadening temperature-dependence errors may induce error in the WMS model	Measure the parameters under controlled laboratory conditions [39]
2. Laser tuning characteristics	Error in the laboratory-measured laser tuning characteristics (modulation amplitude, etc.) may induce error in the WMS model	Do not adjust laser operation settings after measuring tuning characteristics
3. Simulation/experiment wavelength matching	The wavelength between the simulation and experiment must be matched (e.g., at the absorption-feature peak) to accurately compare the model and simulation	Use laser line-locking technique (adaptations of [46,47]), or scan over peak of absorption feature (see Section 5)
4. Background absorption	Background absorption not included in the WMS model will affect the inferred gas properties	Eliminate background absorption or stabilize, measure, and subtract from measured WMS signals
5. Etalon effects	Constructive/destructive interference arising from internal reflections off parallel faces in the optical path can induce errors in the measured WMS signals	Avoid by eliminating parallel surfaces
6. WMS model	If the assumptions in the WMS model do not match the experimental conditions, error may be induced in the model	Ensure experimental conditions match model assumptions
7. Pressure deviation between simulation and experiment	For certain measurement conditions, the pressure will affect the line shape and WMS model, therefore, deviation between the simulated/experimental conditions may induce error in the inferred gas properties	See Subsection 3.A
8. Optical depth and concentration deviation between simulation and experiment	Large optical depths (absorbance>0.05) reduce linearity of the concentration measurement, therefore deviation between the simulated/experimental conditions may induce error in the inferred concentration	See Subsection 3.B

linear pressure dependence that enables the measurement of concentration), but there is also a "non-ideal" pressure effect introduced through the line shape (which is pressure dependent) in the integrand of the equation. The effects of the laser-modulation amplitude are also contained in this integrand. Therefore, the influence of line shape and modulation amplitude on the $2f$ signal can be understood by studying the line-shape integral.

Figure 2 shows the simulated line-shape integral term as a function of modulation index for a Voigt profile with different Lorentzian-width/Doppler-width (L/D) ratios. The Voigt function was used so that the calculated integral is normalized and only needs to be multiplied by the line-center Doppler magnitude to get the actual value of the line-shape integral for any feature. The modulation index is defined as $m = a/\Delta\nu$ (where a is the modulation amplitude and $\Delta\nu$ is the half-width at half-maximum of the absorption feature), and is also used here so that Fig. 2 is generalized for any feature. One can immediately see from the figure that the maximum $2f$ signal occurs near a modulation index of 2.2 for a wide range of L/D (i.e., from Doppler-dominated line shapes all the way to Lorentzian-dominated line shapes). This same conclusion was shown by Reid and Labrie [34]. However, unlike Reid and Labrie, we have used a generalized Voigt line-shape integral for the full range of L/D ratios (instead of pure Lorentzian or Doppler line shapes with different normalizations) to show the large effect that L/D has on the overall $2f$ magnitude, even at $m = 2.2$.

To understand the uncertainty that arises in our $2f$ signal if there is an uncertainty in pressure in the measurement environment, we calculate the effect of a small change in pressure on the $2f$ line-shape integral. A variation in the pressure affects the Lorentzian line width, which changes both the modulation index and L/D. Figure 3 shows the

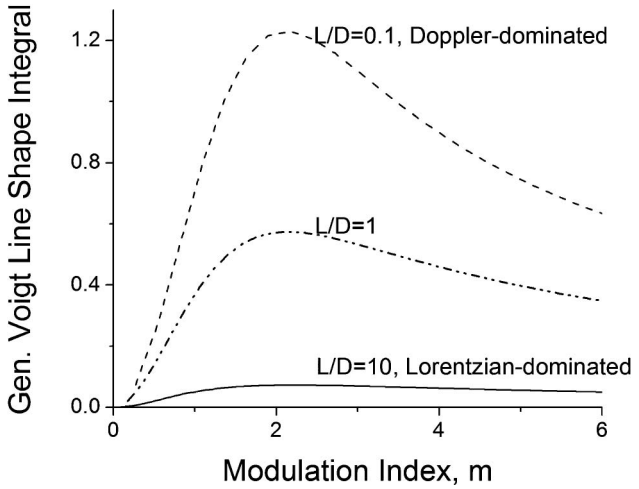

Fig. 2. $2f$ Voigt line-shape integral from Eq. (10) for various Lorentzian-width/Doppler-width (L/D) ratios. Though the peak signal is achieved near $m = 2.2$ for all line-shape profiles, the magnitude of the signals varies significantly.

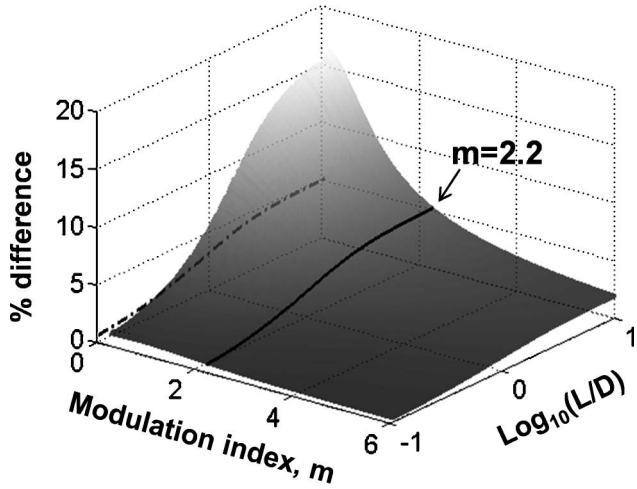

Fig. 3. Percent difference in $2f$ line-shape integral for a -5% change in pressure. L/D = Lorentzian-width/Doppler-width. For isolated, optically thin absorption transitions, this translates directly into percent difference in the $2f$ signal.

percent difference in the $2f$ line-shape integral for a -5% change in pressure plotted versus the starting modulation index and L/D (i.e., before the 5% change in pressure is applied). The black curve represents the percent difference at $m = 2.2$, which is also projected on the modulation index origin plane. For an isolated, optically thin absorption feature and linear laser modulation, this difference translates directly into the percent difference in the $2f$ signal Eq. (10). Thus, if there is a 5% uncertainty between the pressure used to generate the WMS model and the actual pressure in the environment (due to uncertainty in the pressure measurement, pressure variation along the laser LOS, etc.), the percent difference translates into the uncertainty in the WMS signal and potentially the uncertainty in a concentration measurement if the $2f$ signal is used for this purpose.

For more complex cases, the translation is not direct but Fig. 3 still offers an approximation of what one can expect and allows several important conclusions to be drawn. For small L/D, where the Doppler component of the broadening dominates, there is very little difference in the $2f$ signal with pressure change. The difference increases with L/D, and appears to asymptote above $L/D = 10$ for $m = 2.2$. Most importantly, we can see that overmodulation ($m > 2.2$) reduces the difference in the line-shape integral due to pressure change. This suggests that, for cases where ample signal is available, one may choose to overmodulate to reduce uncertainty in concentration measurements at the expense of signal magnitude.

It is also important to understand how changes in pressure affect the ratio of $2f$ signals, because this ratio is used to infer temperature. Figure 4 shows the percent difference in the ratio of $2f$ line-shape integrals due to a -5% change in pressure, plotted against the starting modulation index and L/D ratio (i.e., before the 5% change in pressure is applied). The L/D ratio is defined as the ratio of L/D for two features, where L/D for feature 2 is unity:

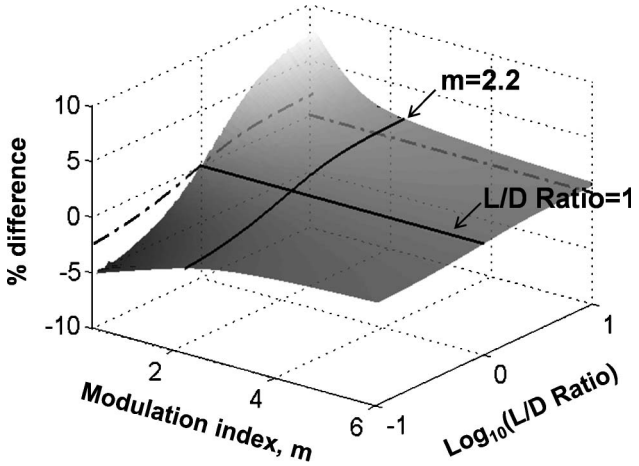

Fig. 4. Percent difference in the ratio of $2f$ line-shape integrals for two absorption features for a −5% change in pressure. L/D Ratio is defined as $((L/D)_{\text{feature 1}}/[(L/D)_{\text{feature 2}} = 1]$.

$$L/D \text{ ratio} = \frac{(L/D)_{\text{feature 1}}}{(L/D)_{\text{feature 2}} = 1}. \tag{13}$$

The black curves represent the percent difference at the critical values of $m = 2.2$ and L/D Ratio $= 1$, and their respective projections. The percent difference in the ratio of $2f$ line-shape integrals does not translate directly to temperature uncertainty due to the nonlinear relationship between the ratio of $2f$ signals and gas temperature. However, Fig. 4 qualitatively illustrates how pressure uncertainty between the simulated WMS model conditions and the actual experimental conditions relates to uncertainty in the ratio of $2f$ signals and, in turn, the inferred temperature.

Two important conclusions are drawn from Fig. 4. First, overmodulation reduces the dependence of the ratio of $2f$ signals on pressure, thus reducing the need for accurate knowledge of pressure. Second, choosing absorption features with similar broadening parameters (so that they have an L/D ratio ~ 1) greatly reduces the influence of pressure. This is because changes in pressure affect both absorption features similarly and, thus, changes in the line-shape integral will cancel when the ratio is taken.

B. Optical Depth

Under many circumstances, absorption features can be selected that are within the linear, optically thin region of absorbance (absorbance <0.05). However, increasing the optical thickness is a good way to increase the $2f$ signal for harsh environments where more signal is needed (except at very large absorbances where the $2f$ signal decreases [40]). Calibration-free WMS using the method and models of Section 2 is still applicable to these non-optically thin cases, provided that one is aware of the underlying assumptions.

To calculate species concentration using Eq. (12), it is implicitly assumed that the $2f$ signal is directly proportional to the concentration. However, at larger optical depths, this assumption becomes less valid because the exponential in Eqs. (4) and (5) cannot be linearized in the same way that it can for the optically thin condition. This breakdown in linearity leads to errors in the calculated species concentration if the simulated species concentration deviates greatly from the true species concentration in the environment. Figure 5 shows the error in the measured species partial pressure using Eq. (12) that is caused by deviation between the true partial pressure and the simulated partial pressure for different optical depths (denoted by absorbance). This figure is specific to the H_2O absorption feature at 7185.6 cm^{-1}, when the simulated H_2O mole fraction is $x = 0.010$ and the true mole fraction is varied between $x = 0.010$ and $x = 0.012$ (holding the total pressure constant). However, the important message from Fig. 5 is that the error induced by a deviation in partial pressure is small in the optically thin limit and steadily increases with absorbance. Thus, for optically thick conditions, the simulations must be performed as close to the expected condition as possible, which may require iteration to draw the simulations acceptably close to an unknown measurement condition.

4. Wavelength-Modulation Spectroscopy Experimental Setup—Hybrid Demultiplexing of Multiple-Wavelength Beams

This section describes an example calibration-free WMS experimental setup based on near-infrared distributed feedback (DFB) diode lasers that is used by our group for measurements in harsh environments. The setup is based on a hybrid combination of wavelength and frequency demultiplexing that

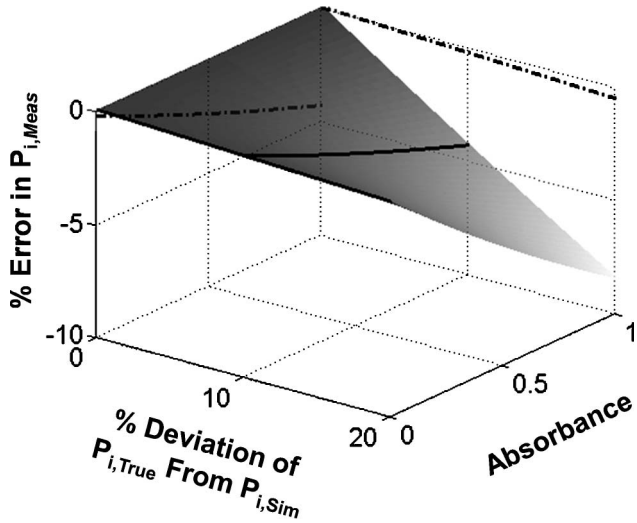

Fig. 5. Error induced in partial pressure measurement using Eq. (12) due to deviation between the true partial pressure and the simulated partial pressure as a function of absorbance (optical depth). Error increases as the true condition deviates from the simulated condition used to calculate the measured partial pressure, and as optical depth increases. Simulation conditions: H_2O absorption feature at 7185.6 cm^{-1} when the simulated H_2O mole fraction is $x = 0.010$ and the true mole fraction is varied between $x = 0.010$ and $x = 0.012$ (holding the total pressure constant).

has the potential to probe a large number of absorption features and species while reducing the complexity of traditional demultiplexing systems. This section discusses the system and optical components, as well as optimization of the laser-modulation parameters.

A. Hybrid Demultiplexing

It is important in many applications to probe absorption at multiple wavelengths either to gain information about multiple species in the system, achieve good temperature sensitivity over a large range of conditions, or gain information about temperature and species nonuniformity along the laser LOS [41–43].

In traditional multiwavelength direct-absorption sensors using DFB diode lasers, the various wavelengths of light are either wavelength- or time-demultiplexed. In time-demultiplexed systems, each laser is turned on in series, so that the resulting detector signal is comprised of each laser signal in sequence. This method offers hardware simplicity at the expense of time response and temporal accuracy. Wavelength-multiplexed systems combine all of the laser wavelengths into a single beam and use a grating located after the light passes through the measurement region to spatially separate each wavelength onto a separate detector. This method solves the temporal issues of time demultiplexing at the expense of hardware complexity and the need to choose wavelengths of sufficient spectral separation that they can be successfully separated by the grating.

WMS offers another possibility—frequency demultiplexing [44]. In this method, each laser is modulated with a different frequency, and the lock-in amplifiers separate the $2f$ and $1f$ signals of each laser from the same detector signal based on the modulation frequency. The method thereby achieves hardware simplicity without giving up fast temporal resolution. However, the number of lasers that can be demultiplexed in this method is somewhat limited (see Subsection 4.B).

As an alternative, we have taken a hybrid-demultiplexing approach, in which wavelength and frequency demultiplexing are combined to separate a large number of signals with reduced complexity. In this scheme, the target absorption features are chosen so that the wavelengths of the tunable diode lasers (TDLs) fall into groups that can be separated onto different detectors after striking a grating. Each laser from a particular group is modulated at a different frequency so that it can be frequency-demultiplexed from the others in that group.

An example setup using this technique is shown in Fig. 6, and was used to obtain the results from a ground-test scramjet engine at the AFRL at WPAFB. shown in subsequent sections. Here, six lasers (NEL America) tuned to H_2O and CO_2 absorption features ranging from 1338 to 1997 nm are multiplexed using a single-mode fiber combiner. A 10 m single-mode

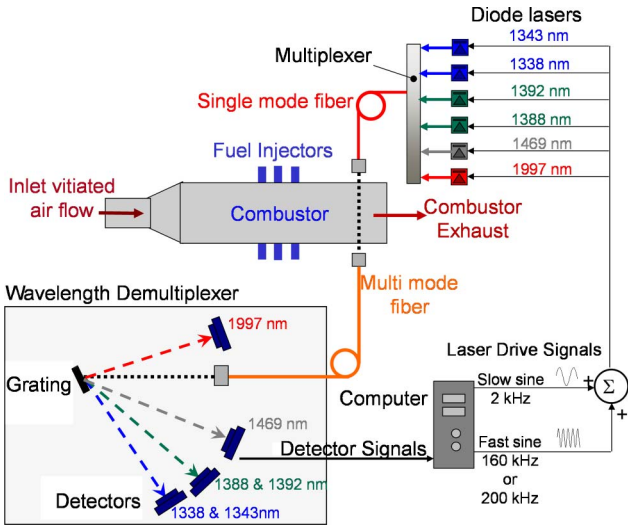

Fig. 6. (Color online) Schematic of hybrid-demultiplexing system configured for the scramjet experiments at AFRL/WPAFB.

fiber (SMF-28) delivers the beam to the scramjet test section, where it is pitched across the combustor exit with an aspheric collimating lens (Thorlabs F240APC-C). After traversing the test region, the beam is collected with a large diameter lens (Oz Optics HPUCO-25-1300-M-10BQ), and focused into a 600 μm multimode fiber. The beam travels through the multimode fiber to the hybrid-demultiplexing setup a few meters from the test section. The light exits the multimode fiber and is collimated by a large diameter aspheric lens (Optosigma 023-2392) onto a 600 grooves/mm diffraction grating (Edmund Optics NT54-851). The dispersed wavelength groups are focused onto separate 3 mm diameter InGaAs photodetectors (Electro-Optical Systems Inc., IGA-030-E5/4 MHz) using a focusing mirror. Each laser in a particular group is modulated at either 160 or 200 kHz for the frequency-demultiplexing step.

All laser drive signal generation and detector output acquisition are performed by one computer using three National Instruments multifunction data acquisition cards (PCI-6115). Phase-insensitive software lock-ins are used to frequency demultiplex the remaining laser groups and recover the $2f$ and $1f$ signals for each laser.

B. Modulation Frequency Optimization

One of the most important aspects of frequency demultiplexing is choosing the laser-modulation parameters to minimize noise and avoid crosstalk between the harmonic signals of the different lasers. It is often helpful to calculate Fourier transforms of the detector signal, such as those shown in Fig. 7 for three different WMS laser-modulation strategies, to study the level of crosstalk and background noise present in a system. Since the lock-in amplifier isolates the signal at the target harmonic plus the region around it that falls within the low-pass filter cutoff of the lock-in, one can use these Fourier

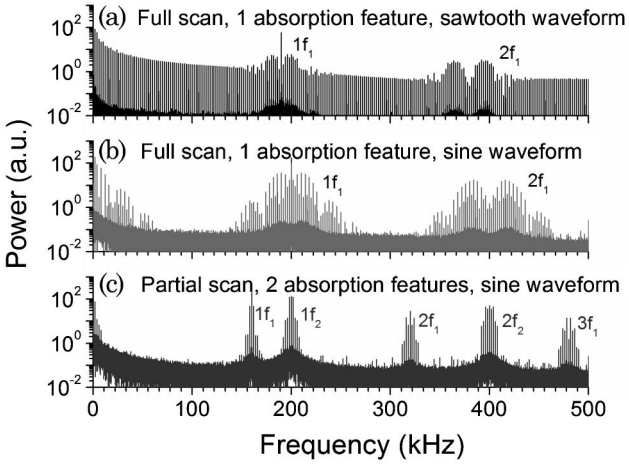

Fig. 7. Fourier transform of detector signals with (a) one laser scanning fully across one absorption feature using a linear ramp waveform, (b) one laser scanning fully across one using a sine waveform, and (c) two lasers scanning across only the peak of two absorption features using a sine waveform. Note in (c) that each laser is modulated at a different frequency so that the harmonic signals for each can be distinguished.

transforms to see what signals are being passed through the lock-in.

In traditional WMS, the laser is modulated with a high-frequency sinusoid that produces the desired $2f$ and $1f$ signals, and a lower frequency linear ramp signal that scans the laser across the absorption feature [this type of modulation strategy is shown in Fig. 1 and the resulting FFT is shown in Fig. 7(a)]. An infinite number of harmonic terms, spaced at the ramp frequency, make up the Fourier transform of a linear ramp waveform. These harmonics, which can be seen as the multitude of features that slowly decrease with increasing frequency in Fig. 7(a), generate noise in the WMS harmonic signals and limit the sensitivity of some WMS signals. To improve the situation, the linear ramp can be replaced with a sine wave, whose Fourier transform is theoretically made up of only a single harmonic at the sinusoid frequency. This improved situation is shown in Fig. 7(b).

In the presence of absorption, scanning the laser across the absorption feature produces sidebands around the modulation frequency and its harmonics. These sidebands, when converted back to the time domain, make up the WMS signals. Thus it is important that these sidebands are captured by the lock-in amplifier and the spacing of these bands determines the minimum low-pass filter frequency that can be used in the lock-in.

For calibration-free WMS measurements, only the $2f$ peak value and the corresponding $1f$ value are important and, therefore, it is only important to scan the laser across the peak of the feature. Reducing the scan range of the laser to only capture the peak also reduces the sideband width and allows a more aggressive low-pass filter step in the lock-in. This, in turn, allows one to add additional lasers and modulation frequencies without interference. This is shown in Fig. 7(c), in which two lasers, one modulated at 160 kHz and the other at 200 kHz, are used to probe an $\sim 0.05\,\mathrm{cm}^{-1}$ window around each peak of two absorption features. The scan range of the laser across the peak should be chosen to ensure that the $2f$ peak of the feature is captured despite changes in peak location due to pressure shift, or slight wavelength drifts of the laser with time.

5. Example Results: CO_2/H_2O Concentration in a Vitiated Supersonic Flow

The sensor system described in Section 4 was applied to a direct-connect, ground-test scramjet combustor at AFRL/WPAFB to measure temperature, H_2O, and CO_2 under a variety of operating conditions. One such condition that was used to test the sensor system was with only the supersonic flow from the vitiated air heater passing through the combustor duct. The vitiator consists of a lean methane and air combustion chamber upstream of the expansion nozzle at the entrance to the scramjet test section. The vitiator increases the incoming air temperature to ensure that the proper scramjet inlet conditions are met when the supersonic flow is generated in the expansion nozzle. The lean methane/air mixture produces a well-known H_2O/CO_2 ratio.

Details on the ground-test scramjet test facility at AFRL/WPAFB can be found in [30] and details on the scramjet flow path and measurement location can be found in [13]. The laser beam passes through the scramjet downstream of the flame holders in an expanding section of the duct. The approximate static pressure at the measurement location for the vitiator-only condition was 0.26 atm with a static temperature around 600 K. The sensor was tested using both direct-absorption and calibration-free WMS to probe absorption on the R50 transition of the 20012←00001 band of CO_2 near $5007.8\,\mathrm{cm}^{-1}$. This transition is relatively free of water-vapor interference and has a lower-state energy (E'') of $994\,\mathrm{cm}^{-1}$, which makes it suitable for measurements in this temperature range. The sensor probes five transitions of water vapor with a large variety of lower-state energies: near $6807.8\,\mathrm{cm}^{-1}$ ($E'' = 3319\,\mathrm{cm}^{-1}$), $7185.6\,\mathrm{cm}^{-1}$ ($E'' = 1045\,\mathrm{cm}^{-1}$), $7205.2\,\mathrm{cm}^{-1}$ ($E'' = 79\,\mathrm{cm}^{-1}$), $7444.4\,\mathrm{cm}^{-1}$ ($E'' = 1790\,\mathrm{cm}^{-1}$), and $7472.2\,\mathrm{cm}^{-1}$ ($E'' = 2952\,\mathrm{cm}^{-1}$). This wide range of lower-state energies allows sensitive measurements over a variety of temperature conditions. The feature near $7185.6\,\mathrm{cm}^{-1}$ was used for the water-vapor measurements in the temperature range of the vitiator-only condition.

Figure 8 shows representative results of the H_2O and CO_2 measurements. Figures 8(a) and 8(c) show a single scan of CO_2 absorption using (a) WMS-$2f$ and (c) direct absorption on consecutive runs of the scramjet. The WMS signal appears smooth compared to the direct absorption because the lock-in amplifier rejects $1/f$ laser noise and electronic noise. Only the peak of the feature is scanned, and the line shape appears distorted near the beginning and end of the scan

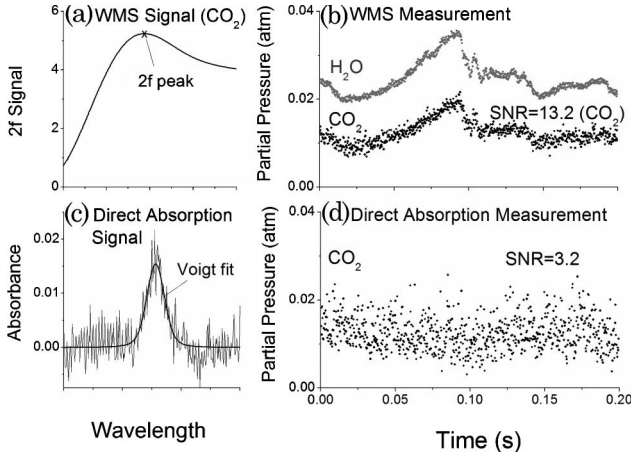

Fig. 8. Comparison of direct absorption and 2*f* signals and CO_2 partial pressure measurements in a vitiated supersonic flow using an absorption feature of CO_2 near 1997 nm. The left panels show single-scan data with (a) the WMS-2*f* and (c) direct-absorption techniques, along with the peak or Voigt fit values that are used to calculate the CO_2 concentration (the wavelength scales are different for the two figures). The right panels show the measured CO_2 partial pressure at 4 kHz using (b) 2*f* peak magnitudes and (d) integrated absorbances.

due to the sinousoidal waveform used (instead of a linear ramp). Also shown are the 2*f* peak value and the Voigt fit. The 2*f* peak value and the integrated absorbance extracted from the Voigt fit are used to infer the CO_2 concentration with the WMS and direct-absorption methods, respectively. Figures 8(b) and 8(d) show the measured concentrations in terms of partial pressures for a 0.2 s time period using both of these methods. The measurement rate is 4 kHz. Although the WMS and direct-absorption data are taken from different scramjet runs and, thus, are not expected to have identical fluctuation patterns, one can see that the higher SNR of the WMS technique is capable of resolving rapid fluctuations in this flow that may be obscured by the lower SNR of the direct-absorption measurement.

The SNR was calculated from the partial pressure data and is defined as the ratio of the mean partial pressure divided by the standard deviation (after a 200 Hz high-pass filter is used to remove the actual fluctuations in the system). The SNR of the calibration-free WMS measurement (13.2) is 4× better than the direct-absorption measurement (3.2). From the single-scan data shown in Figures 8(a) and 8(c) one might expect the difference in SNR to be even larger; however, the SNR of the direct-absorption measurement benefits from the use of a Voigt fit while the WMS relies on a single (peak) point. The SNR obtained with the WMS measurements is excellent considering the low CO_2 absorbance levels (<2%) and the supersonic nature of the flow.

In terms of concentration levels, the measured H_2O/CO_2 ratio using calibration-free WMS is 1.99, which is within 0.5% of the expected value of 2.00 for the methane–air vitiated heater.

Taken together, these results confirm the SNR benefits of WMS and show that accurate results can be obtained with WMS without on-site calibration.

6. Example Results: Comparison Between Line-of-Sight Laser Measurement and Two-Dimensional Computational Fluid Dynamics in Combusting Supersonic Flow

An important consideration for laser-absorption measurements in harsh environments is the path-integrated nature of the measured quantities, which can be difficult to interpret when the quantities are nonuniform along the beam path. The absorption signal for every absorption feature has a different, nonlinear response to temperature that is determined by the feature's lower-state energy (E''). For a laser path with nonuniform temperature, this nonlinear absorption behavior of each feature will cause the temperature inferred from various pairs of absorption features to differ. Thus, the inferred temperature from a laser measurement in a nonuniform environment is not simply equal to the path-averaged temperature [41], making direct comparison of LOS laser measurements with multidimensional CFD more difficult.

Two general methods have been proposed to enable the comparison. The temperature profile method first suggested by Sanders *et al.* [42] and explored further in [43] uses the CFD to prescribe a general temperature profile with several key characteristics (e.g., T_{wall}, T_{peak}, etc.) that can be solved from the measured absorption of several absorption features with unique temperature dependence. This method is difficult to apply in harsh, practical environments because a large number of features must be probed to accurately determine the nonuniform profile (particularly for complex profiles), and because measurement noise can affect convergence of the results. In addition, the influence of pressure and mole fraction on the calibration-free WMS signals further complicates data processing and the accuracy of the results.

A simpler method was suggested and applied in [45], which uses the CFD in combination with the WMS model presented above to calculate the expected WMS signals that would result from a hypothetical laser measurement through the CFD. The expected signals are then treated like the measured signals and compared with the WMS model to infer the expected laser-measured temperature for the CFD. In this way, the effect of nonuniformity on the nonlinear absorption response of the probed spectral features will be included in both the measurement and the CFD-calculated expected temperature, and the results can be directly compared.

This technique is much simpler to implement than the temperature-profiling method because it requires only two absorption features, which significantly reduces hardware and software complexity. The drawback to this technique is that it reduces the nonuniform temperature along the laser LOS to a single value, which helps to understand how

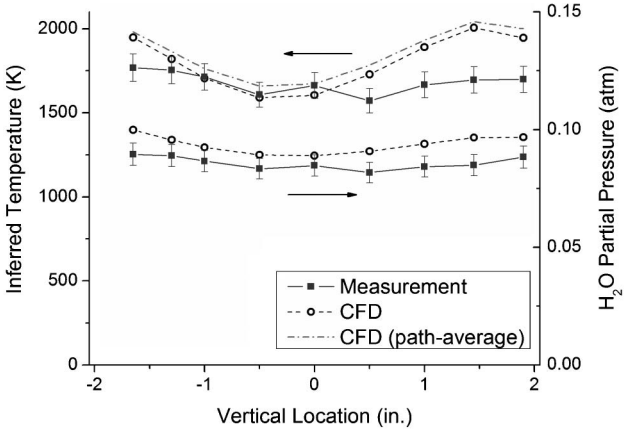

Fig. 9. Static temperature and H_2O partial pressure for different vertical locations in the scramjet combustor during full operation on ethylene and air. Each point is the LOS laser-measured value for the experiment (solid squares) and the expected LOS laser-measured value from the CFD-calculated flow field (open circles). The gray curve (no symbols) represents the path-average temperature from the CFD-calculated flow field.

accurately the CFD model is predicting the actual temperature profile, but does not recover specific regions of the nonuniform profile.

Some example results using this method are shown in Fig. 9 for the scramjet combustor at AFRL/WPAFB under full operation on ethylene and air at an equivalence ratio of $\phi = 0.7$. The laser-measured temperature and H_2O partial pressure were inferred using calibration-free WMS on the $6807.8\,cm^{-1}$ ($E'' = 3319\,cm^{-1}$) and $7185.6\,cm^{-1}$ ($E'' = 1045\,cm^{-1}$) features at several vertical locations in the combustor duct (represented by the solid squares). The expected laser-measured values based on three-dimensional (3D) CFD calculations of the flow field are represented by the open circles. Figure 9 also shows the regular path-average temperature based on the 3D CFD (gray curve, no symbols). Though the expected laser-measured temperature is different than the path-average temperature, the trends are retained very well and show that information about the path-average temperature can be gained from the laser-measured temperature.

The uncertainty bars shown on the experimentally-measured values are the compound result of the uncertainty estimate in Table 2, which follows from the discussion on potential sources of uncertainty in Section 3.

By obtaining data from several vertical locations, some information about the nonuniform gas properties in the combustor can be retained. For example, the temperature from the sensor measurement and the CFD agree well in the core flow region (within 4%). The measurements also indicate a lower temperature than expected near the top and bottom wall of the combustor. These results suggest that the CFD is underpredicting mass and/or energy transport. The H_2O partial pressure measurements in the combustor are ~5–12% lower than predicted by the CFD, which may also indicate that OH to H_2O conversion rate is overpredicted by CFD. For more extensive results and discussion, see [45].

7. Summary and Conclusions

A method was presented for direct comparison of WMS measurements with WMS models to infer gas temperature and concentration. The method uses laser sources with synchronous wavelength and intensity modulation, which give rise to a $1f$ signal that can be used to normalize the $2f$ signal for laser intensity. Including laser-specific tuning characteristics and precise spectral data in the WMS model allows the model and measurement to be directly compared, eliminating the need for on-site calibration using a known mixture or operating condition.

Table 2. Estimated Uncertainty for Calibration-Free Wavelength-Modulation Spectroscopy Measurements in the Scramjet Combustor at AFRL/WPAFB

Source of Uncertainty	Estimated Uncertainty in T_{Meas}	Estimated Uncertainty in $P_{H_2O,Meas}$	Comment
1. Spectral parameters 2. Laser tuning characteristics	+/− 4.2%	+/− 2.7%	Estimated from laboratory validation in a controlled furnace and a uniform flame [45]
3. Simulation/experiment wavelength matching	Negligible	Negligible	Accounted for by scanning absorption-feature peak and matching experiment/simulation at peak wavelength
4. Background absorption	Negligible	Negligible	Steady N_2 purge + background subtraction of residual
5. Etalon effects	Negligible	Negligible	Eliminated by angle-polished fibers and three wedges on all windows
6. WMS model	Negligible	Negligible	Model was properly matched to the experiment
7. Pressure deviation between simulation and experiment	+/− 0.35%	+/− 1.75%	Estimated from simulations based on actual measured pressure variation and CFD-predicted pressure nonuniformity
8. Optical depth and concentration deviation between simulation and experiment	+/− 0.06%	+/− 0.9%	Estimated from simulations based on CFD-predicted concentration nonuniformity
Total	+/− 4.6%	+/− 5.4%	

The uncertainties associated with calibration-free WMS in harsh environments were summarized, and it was shown that pressure can have an important effect on the magnitude of $2f$ signals by influencing line shape. The influence of pressure was studied, yielding the following design rules to aid in optimization of the sensor.

1. If the pressure and the nominal species concentration are accurately known and incorporated in the simulations, wavelength modulation at modulation index $m = 2.2$ can be used to maximize the $2f$ signal.
2. If pressure is not well known in the measurement environment, a modulation index $m > 2.2$ should be used to reduce error induced by pressure uncertainty. For temperature measurements, choosing features with similar L/D (Lorentzian-width-to-Doppler-width ratio) and broadening parameters further reduces errors associated with pressure uncertainty.

The effect of absorption-feature optical depth on the calibration-free WMS method and uncertainty was also studied. By choosing absorption features with greater optical depth, it is possible to increase the $2f$ signal strength and improve SNR; however, this can lead to increased error if the nominal pressure and mole fraction are not well known (iteration may be necessary when comparing the measurements and model to infer gas properties).

A hybrid system that combines wavelength and frequency demultiplexing to distinguish six lasers probing H_2O and CO_2 transitions from 1.3 to 2.0 μm was shown. The laser-modulation parameters were investigated to determine the optimal combination for frequency demultiplexing with low noise. It was found that a sine wave that only scans the laser over the absorption-feature peak (instead of a linear ramp that scans across the entire feature) is the optimal waveform for the low-frequency laser scan modulation (not to be confused with the modulation at $1f$, which is always sinusoidal).

The system was applied to a direct-connect, ground-test scramjet combustor at AFRL/WPAFB to measure H_2O, CO_2, and temperature. Measurements of CO_2 using both direct absorption and $1f$-normalized, WMS-$2f$ at the same operating condition showed a 4× increase in SNR for the WMS measurements. The measured H_2O/CO_2 ratio for this condition was within 0.5% of the expected ratio. A cut of 3D CFD at the laser beam location was compared with the LOS temperature and H_2O measurements during full scramjet operation using a method that takes into account the effect of LOS nonuniformity on the absorption measurements. The comparisons demonstrate the usefulness of the calibration-free measurements to elucidate information about multidimensional CFD.

Overall, this paper provides a guide and demonstration of the calibration-free WMS technique, and may open the door to practical implementation of WMS in a variety of new harsh, real-world environments.

This research was sponsored by the Air Force Office of Scientific Research (AFOSR), Aerospace and Materials Directorate, with Julian Tishkoff as technical monitor. The authors thank Mark Gruber, Tarun Mathur, and Cam Carter, of AFRL/WPAFB, and Andrew Fahrland and Andree Houle of Stanford University for making the demonstrations at AFRL possible. The authors also thank Jiwen Liu of AFRL/WPAFB for providing the CFD calculations.

References and Notes

1. E. D. Hinkley and P. L. Kelley, "Detection of air pollutants with tunable diode lasers," Science **171**, 635–639 (1971).
2. R. K. Hanson and P. K. Falcone, "Temperature measurement technique for high temperature gases using a tunable diode laser," Appl. Opt. **17**, 2477–2480 (1978).
3. M. Lackner, "Tunable diode laser spectroscopy (TDLAS) in the process industries—a review," Rev. Chem. Eng. **23**, 65 (2007).
4. P. A. Martin, "Near-infrared diode laser spectroscopy in chemical process and environmental air monitoring," Chem. Soc. Rev. **31**, 201–210 (2002).
5. P. Werle, "A review of recent advances in semiconductor laser based gas monitors," Spectrochim. Acta **54**, 197–236 (1998).
6. M. G. Allen, "Diode laser absorption sensors for gas-dynamic and combustion flows," Meas. Sci. Technol. **9**, 545–562 (1998).
7. R. K. Hanson and J. B. Jeffries, "Diode laser sensors for ground testing," in *Proceedings of the Twenty-Fifth American Institute of Aeronautics and Astronautics Aerodynamic Measurement Technology and Ground Testing Conference*, AIAA 2006-3441 (American Institute of Aeronautics and Astronautics, 2006).
8. We refer here to the frequency of the modulation sinusoid, not the modulation amplitude (which is sometimes also reported in frequency units).
9. J. A. Silver, "Frequency-modulation spectroscopy for trace species detection: theory and comparison among experimental methods," Appl. Opt. **31**, 707–717 (1992).
10. D. S. Bomse, A. C. Stanton, and J. A. Silver, "Frequency modulation and wavelength modulation spectroscopies: comparison of experimental methods using a lead-salt diode laser," Appl. Opt. **31**, 718–731 (1992).
11. T. Fernholz, H. Teichert, and V. Ebert, "Digital, phase-sensitive detection for in situ diode-laser spectroscopy under rapidly changing transmission conditions," Appl. Phys. B **75**, 229–236 (2002).
12. J. T. C. Liu, G. B. Rieker, J. B. Jeffries, M. R. Gruber, C. D. Carter, T. Mathur, and R. K. Hanson, "Near-infrared diode laser absorption diagnostic for temperature and water vapor in a scramjet combustor," Appl. Opt. **44**, 6701–6711 (2005).
13. G. B. Rieker, J. B. Jeffries, R. K. Hanson, T. Mathur, M. R. Gruber, and C. D. Carter, "Diode laser-based detection of combustor instabilities with application to a scramjet engine," Proc. Combust. Inst. **32**, 831–838 (2009).
14. G. B. Rieker, H. Li, X. Liu, J. T. C. Liu, J. B. Jeffries, R. K. Hanson, M. G. Allen, S. D. Wehe, P. A. Mulhall, H. S. Kindle, A. Kakuho, K. R. Sholes, T. Matsuura, and S. Takatani, "Rapid measurements of temperature and H_2O concentration in IC engines with a spark plug-mounted diode laser sensor," Proc. Combust. Inst. **31**, 3041–3049 (2007).
15. J. Gustafsson, N. Chekalin, and O. Axner, "Improved detectability of wavelength modulation diode laser absorption spectrometry applied to window-equipped graphite furnaces by

4th and 6th harmonic detection," Spectrochim. Acta B **58**, 111–122 (2003).
16. R. T. Wainner, B. D. Green, M. G. Allen, M. A. White, J. Stafford-Evans, and R. Naper, "Handheld, battery-powered near-IR TDL sensor for stand-off detection of gas and vapor plumes," Appl. Phys. B **75**, 249–254 (2002).
17. J. A. Silver and D. J. Kane, "Diode laser measurements of concentration and temperature in microgravity combustion," Meas. Sci. Technol. **10**, 845–852 (1999).
18. S. Hunsmann, K. Wunderle, S. Wagner, U. Rascher, U. Schurr, and V. Ebert, "Absolute, high resolution water transpiration rate measurements on single plant leaves via tunable diode laser absorption spectroscopy (TDLAS) at 1.37 mm," Appl. Phys. B **92**, 393–401 (2008).
19. J. Henningsen and H. Simonsen, "Quantitative wavelength-modulation without certified gas mixtures," Appl. Phys. B **70**, 627–633 (2000).
20. K. Duffin, A. J. McGettrick, W. Johnstone, G. Stewart, and D. G. Moodie, "Tunable diode laser spectroscopy with wavelength modulation: a calibration-free approach to the recovery of absolute gas absorption line-shapes," J. Lightwave Technol. **25**, 3114–3125 (2007).
21. A. J. McGettrick, K. Duffin, W. Johnstone, G. Stewart, and D. G. Moodie, "Tunable diode laser spectroscopy with wavelength modulation: a phasor decomposition method for calibration-free measurements of gas concentration and pressure," J. Lightwave Technol. **26**, 432–440 (2008).
22. D. T. Cassidy and J. Reid, "Atmospheric pressure monitoring of trace gases using tunable diode lasers," Appl. Opt. **21**, 1185–1190 (1982).
23. K. Uehara and H. Tai, "Remote detection of methane with a 1.66 μm diode laser," Appl. Opt. **31**, 809–814 (1992).
24. T. Iseki, H. Tai, and K. Kimura, "A portable remote methane sensor using a tunable diode laser," Meas. Sci. Technol. **11**, 594–602 (2000).
25. H. Li, G. B. Rieker, X. Liu, J. B. Jeffries, and R. K. Hanson, "Extension of wavelength-modulation spectroscopy to large modulation depth for diode laser absorption measurements in high-pressure gases," Appl. Opt. **45**, 1052–1060 (2006).
26. L. S. Rothman, D. Jacquemart, A. Barbe, D. C. Benner, M. Birk, L. R. Brown, M. R. Carleer, C. Chackerian, Jr., K. Chance, L. H. Coudert, V. Dana, V. M. Devi, J. M. Flaud, R. R. Gamache, A. Goldman, J. M. Hartmann, K. W. Jucks, A. G. Maki, J. Y. Mandin, S. T. Massie, J. Orphal, A. Perrin, C. P. Rinsland, M. A. H. Smith, J. Tennyson, R. N. Tolchenov, R. A. Toth, J. Vander Auwera, P. Varanasi, and G. Wagner, "The HITRAN 2004 molecular spectroscopic database," J. Quant. Spectrosc. Radiat. Transfer **96**, 139–204 (2005).
27. G. B. Rieker, X. Liu, H. Li, J. B. Jeffries, and R. K. Hanson, "Measurements of near-IR water vapor absorption at high pressure and temperature," Appl. Phys. B **87**, 169–178 (2007).
28. G. B. Rieker, J. B. Jeffries, and R. K. Hanson, "Measurements of high-pressure CO_2 absorption near 2.0 mm and implications on tunable diode laser sensor design," Appl. Phys. B **94**, 51–63 (2009).
29. G. B. Rieker, H. Li, X. Liu, J. B. Jeffries, R. K. Hanson, M. G. Allen, S. D. Wehe, P. A. Mulhall, and H. S. Kindle, "A diode laser sensor for rapid, sensitive measurements of gas temperature and water vapour concentration at high temperatures and pressures," Meas. Sci. Technol. **18**, 1195–1204 (2007).
30. M. R. Gruber, J. Donbar, K. Jackson, T. Mathur, R. Baurle, D. Eklund, and C. Smith, "Newly developed direct-connect high-enthalpy supersonic combustion research facility," J. Propul. Power **17**, 1296–1304 (2001).
31. $\cos(\alpha)$ represents a frequency component of the detector signal and $\cos(\beta)$ represents the reference sinusoid. If β is chosen to be $2\pi f_o t$, where $f_o = 2f$, then the frequency components of the detector signal with $\alpha \approx \beta$ (i.e., components near $2f$) will be shifted to $\alpha - \beta \approx 0$, and become the DC output of the lock-in.
32. J. H. Scofield, "A frequency-domain description of a lock-in amplifier," Am. J. Phys. **62**, 129–133 (1994).
33. P. Kluczynski and O. Axner, "Theoretical description based on Fourier analysis of wavelength-modulation spectrometry in terms of analytical and background signals," Appl. Opt. **38**, 5803–5815 (1999).
34. J. Reid and D. Labrie, "Second-harmonic detection with tunable diode lasers—comparison of experiment and theory," Appl. Phys. B **26**, 203–210 (1981).
35. L. C. Philippe and R. K. Hanson, "Laser diode wavelength-modulation spectroscopy for simultaneous measurement of temperature, pressure, and velocity in shock-heated oxygen flows," Appl. Opt. **32**, 6090–6103 (1993).
36. J. T. C. Liu, J. B. Jeffries, and R. K. Hanson, "Wavelength modulation absorption spectroscopy with 2*f* detection using multiplexed diode lasers for rapid temperature measurements in gaseous flows," Appl. Phys. B **78**, 503–511 (2004).
37. P. Kluczynski, J. Gustafsson, A. M. Lindberg, and O. Axner, "Wavlength modulation absorption spectrometry—an extensive scrutiny of the generation of signals," Spectrochim. Acta B **56**, 1277–1354 (2001).
38. S. Schilt, L. Thevenaz, and P. Robert, "Wavelength modulation spectroscopy: combined frequency and intensity laser modulation," Appl. Opt. **42**, 6728–6738 (2003).
39. X. Liu, J. B. Jeffries, and R. K. Hanson, "Measurements of spectral parameters of water-vapour transitions near 1388 and 1345 nm for accurate simulation of high-pressure absorption spectra," Meas. Sci. Technol. **18**, 1185–1194 (2007).
40. O. Axner, J. Gustafsson, F. M. Schmidt, N. Omenetto, and J. D. Winefordner, "A discussion about the significance of absorbance and sample optical thickness in conventional spectrometry and wavelength-modulated laser absorption spectrometry," Spectrochim. Acta B Spectrochim. Acta B**58**, 1997–2014 (2003).
41. J. M. Seitzman and B. T. Scully, "Broadband infrared absorption sensor for high-pressure combustor control," J. Propul. Power **16**, 994–1001 (2000).
42. S. T. Sanders, J. Wang, J. B. Jeffries, and R. K. Hanson, "Diode-laser absorption sensor for line-of-sight gas temperature distributions," Appl. Opt. **40**, 4404–4415 (2001).
43. X. Liu, J. B. Jeffries, and R. K. Hanson, "Measurement of non-uniform temperature distributions using line-of-sight absorption spectroscopy," AIAA J. **45**, 411–419 (2007).
44. D. B. Oh, M. E. Paige, and D. S. Bomse, "Frequency modulation multiplexing for simultaneous detection of multiple gases by use of wavelength modulation spectroscopy with diode lasers," Appl. Opt. **37**, 2499–2501 (1998).
45. M. R. Gruber, C. D. Carter, M. Ryan, G. B. Rieker, J. B. Jeffries, R. K. Hanson, J. Liu, and T. Mathur, "Laser-based measurements of OH, temperature, and water vapor concentration in a hydrocarbon-fueled scramjet," in *Proceedings of Forty-Fourth American Institute of Aeronautics and Astronautics/American Society of Mechanical Engineers/Society of Automotive Engineers/American Society for Engineering Education Joint Propulsion Conference and Exhibit*, AIAA 2008-5070 (American Institute of Aeronautics and Astronautics, 2008).
46. G. J. Koch, A. L. Cook, C. M. Fitzgerald, and A. N. Dharamsi, "Frequency stabilization of a diode laser to absorption lines of water vapor in the 944 nm wavelength region," Opt. Eng. **40**, 525–528 (2001).
47. R. Matthey, S. Schilt, D. Werner, C. Affolderbach, L. Thevenaz, and G. Mileti, "Diode laser frequency stabilisation for water-vapour differential absorption sensing," Appl. Phys. B **85**, 477–485 (2006).